

3  
4 **Running title:** ISO's effects on Huh-7 cells

5  
6 **Isoguanosine exerts anticancer effects in Huh-7 cells by modulating ROS-dependent MAPK**  
7 **and AKT signaling**

8  
9 An-Qi Wang<sup>1,#</sup>, Xiao-Yu Jin<sup>2,#</sup>, Ying-Hua Luo<sup>3,#</sup>, Nan Wu<sup>1,4,5</sup>, Yan-Jun Tang<sup>4,5</sup>, Yan-Zhi Liu<sup>1,4,5</sup>,  
10 Tian-Zhu Li<sup>6,\*</sup>, Cheng-Hao Jin<sup>1,4,5,\*</sup>

11  
12 <sup>1</sup>Department of Biochemistry and Molecular Biology, College of Life Science and Biotechnology,  
13 Heilongjiang Bayi Agricultural University, Daqing, China; <sup>2</sup>Department of CT, Daqing Oilfield  
14 General Hospital, Daqing, China; <sup>3</sup>Department of Grass Science, College of Animal Science and  
15 Veterinary Medicine, Heilongjiang Bayi Agricultural University, Daqing, China; <sup>4</sup>Department of  
16 Food Science and Engineering, College of Food Science, Heilongjiang Bayi Agricultural University,  
17 Daqing, China; <sup>5</sup>National Coarse Cereals Engineering Research Center, Daqing, China; <sup>6</sup>  
18 Department of Molecular Biology, College of Basic Medical Science, Chifeng University, Chifeng,  
19 Inner Mongolia Autonomous Region, China

20  
21 \*Correspondence: [jinchenghao3727@byau.edu.cn](mailto:jinchenghao3727@byau.edu.cn); [litianzhu@cfxy.edu.cn](mailto:litianzhu@cfxy.edu.cn)

22  
23 #Contributed equally to this work.

24  
25 **Received December 4, 2025 / Accepted April 9, 2026**

26  
27 Isoguanosine (ISO) is a naturally occurring bioactive compound with multiple pharmacological  
28 properties. In this study, the inhibitory effects of ISO on hepatocellular carcinoma (HCC) cells and  
29 its underlying molecular mechanisms were investigated. The cell viability after ISO treatment was  
30 assessed using the CCK-8 assay, trypan blue staining, and Hoechst 33342/PI double staining. The  
31 relevant targets of ISO and their regulatory mechanisms were predicted using network  
32 pharmacology and molecular docking technology. The induction of apoptosis by ISO on Huh-7  
33 cells was detected by Annexin V-FITC/PI double staining combined with flow cytometry and  
34 western blotting. The cell cycle arrest effect of ISO on Huh-7 cells was detected by Ki-67 staining,  
35 flow cytometry, and western blotting. The migration-inhibition effect of ISO on Huh-7 cells was  
36 detected by the wound healing, Transwell, and western blotting. In addition, the effects of reactive  
37 oxygen species (ROS) and protein kinase B (AKT) on Huh-7 cells were investigated by using  
38 N-acetyl cysteine (NAC) and AKT inhibitor HY10249, respectively. Cell viability assays  
39 demonstrated that ISO exerts a significant cytotoxic effect on HCC cell lines. Network  
40 pharmacology analysis revealed that the core targets of ISO are associated with ROS, AKT, and  
41 mitogen-activated protein kinase (MAPK) signaling pathways. Molecular docking results indicate  
42 that ISO has a strong binding affinity for AKT1, CASP3, and GSK3B. Apoptosis assays indicated  
43 that ISO induces apoptosis in Huh-7 cells via the mitochondria-dependent pathway. Furthermore,  
44 ISO modulates apoptosis through the MAPK and signal transducer and activator of transcription 3  
45 (STAT3) signaling pathways. Cell cycle assays showed that ISO induces G2/M phase arrest by

46 elevating intracellular ROS levels. Migration assays demonstrated that ISO inhibits cell migration  
47 by regulating the AKT signaling pathway. In addition, pretreatment with NAC reversed  
48 ISO-induced apoptosis, cell cycle arrest, and inhibition of migration. ISO promotes apoptosis,  
49 induces cell cycle arrest, and inhibits Huh-7 cell migration. These findings provide a theoretical  
50 basis for further pharmacological research and support the potential development and application of  
51 ISO as an anticancer agent.

52  
53 **Key words:** isoguanosine; hepatocellular carcinoma; cell apoptosis; cell cycle; cell migration; ROS  
54  
55

56 Hepatocellular carcinoma (HCC) is a malignant tumor originating from hepatocytes cells [1], and it  
57 is typically diagnosed at an intermediate or advanced stage [2]. In recent years, the global incidence  
58 and mortality rates of HCC has continued to rise annually [3], posing a serious threat to public  
59 health and human life [4, 5]. Depending on individual clinical circumstances, patients with liver  
60 cancer are commonly treated with surgery, chemotherapy, or radiotherapy [1]. Chemotherapy is a  
61 well-established modality in oncology [6, 7]. However, its efficacy is significantly compromised  
62 due to frequent adverse effects and the growing problem of resistance to chemotherapeutic agents [8,  
63 9]. Therefore, the development of novel and safe antitumor agents for the treatment of HCC is  
64 urgently needed.

65 Naturally derived compounds extracted from traditional Chinese herbal medicines have  
66 demonstrated multi-target and multi-pathway therapeutic effects against various cancers [10-12]. In  
67 recent years, the anti-inflammatory, antibacterial, and antitumor properties of isoguanosine (ISO)  
68 have garnered significant research interest both domestically and internationally [13-15]. However,  
69 studies investigating its efficacy against liver cancer and its precise antitumor mechanisms remain  
70 limited. Thus, this study aimed to elucidate whether ISO exerts inhibitory effects on the growth of  
71 Huh-7 cells and to explore its associated molecular mechanisms.

72 Numerous studies have demonstrated that natural or synthetic compounds can induce diverse forms  
73 of regulated cell death, including cell apoptosis necroptosis, ferroptosis, pyroptosis, and autophagic  
74 cell death, contributing to their anticancer activity [16-18]. A comprehensive understanding of these  
75 pathways is essential for exploring the full anticancer mechanisms of bioactive compounds. In this  
76 study, we focused on elucidating the apoptotic pathway induced by ISO in Huh- 7 cells. Inducing  
77 apoptosis in cancer cells is one of the effective and widely used strategies in cancer treatment  
78 [19-21]. Apoptosis can be initiated through mitochondrial pathways or via activation of death

79 receptors [22, 23]. Reactive oxygen species (ROS), the principal by products of oxidative stress, are  
80 known to contribute to tumor initiation and progression [24, 25]. When excessively accumulated,  
81 ROS can modulate several signaling pathways, most notably the protein kinase B (AKT) and  
82 mitogen-activated protein kinase (MAPK) pathways [26]. These pathways play essential roles in  
83 various biological processes, including cell adhesion, survival, and migration [27, 28]. ROS are also  
84 involved in regulating the activation of signaling pathways such as AKT and the signal transduction  
85 and activator of transcription 3 (STAT3), and may cooperate with the MAPK pathway to promote  
86 apoptosis [29, 30].

87 This study aimed to achieve the following research objectives with corresponding expected  
88 outcomes: The main research objective is to predict the ISO-related targets and the regulatory  
89 effects of ISO on HCC using network pharmacology methods. To achieve this, we first screened  
90 multiple HCC cell lines via the CCK-8 assay and selected Huh-7 cells as the in vitro model for  
91 subsequent experiments. We verified the binding affinity of ISO to its predicted target proteins and  
92 elucidated its anticancer effects (pro-apoptosis, cell cycle regulation, anti-migration) and underlying  
93 molecular mechanisms in Huh-7 cells. Thereby providing a systematic in vitro validation  
94 experimental basis for ISO as a potential new anti-HCC candidate drug. The expected result is to  
95 identify ROS accumulation as the upstream initiating factor for ISO's anti-HCC effect, and ISO  
96 exerts a pro-apoptotic effect by activating the ROS-mediated MAPK/STAT3 signaling pathway to  
97 regulate downstream apoptotic proteins. By inhibiting the AKT signaling pathway, cell cycle arrest  
98 is induced, and the migration of liver cancer cells is inhibited through the GSK-3 $\beta$ / $\beta$ -catenin  
99 signaling pathway. Ultimately, we obtained systematic experimental data on the multi-pathway  
100 regulatory mechanism of ISO on HCC cells, which will lay a solid theoretical and experimental  
101 foundation for further pharmacological research on ISO as an anti-cancer drug and its potential  
102 clinical development and application.

103

## 104 **Materials and methods**

105 **Cell lines and cell culture.** HCC cell lines Huh-7, HepG2, and Hep3B, along with the human  
106 normal lung cell line IMR-90, were obtained from the American Type Culture Collection (ATCC,  
107 Manassas, VA, USA). The human normal stomach cell line GES-1, normal liver cell line THLE-2,  
108 and normal renal cell line 293T were obtained from Sage Biotechnology Co., Ltd. (Shanghai,

109 China). All cell lines were cultured in Dulbecco's Modified Eagle's Medium (DMEM; Gibco,  
110 Waltham, MA, USA), supplemented with 10% fetal bovine serum (FBS; Gibco), 100 U/ml  
111 penicillin, and 100 µg/ml streptomycin (P/S; Gibco). Cells were incubated at 37 °C in a humidified  
112 atmosphere containing 5% CO<sub>2</sub> in a sterile cell incubator (SanYo, Osaka, Japan). The core  
113 experimental model in this study is a hepatocellular carcinoma cell line. The inclusion of normal  
114 cell lines was done for the purpose of conducting specific cytotoxicity comparison assessments. All  
115 cell lines were obtained from ATCC and tested negative for mycoplasma contamination.

116 **Cell viability analysis.** Cell viability was assessed using the Cell Counting Kit-8 (CCK-8; Solarbio,  
117 Beijing, China), 0.4% Trypan Blue Stain Solution (Coolaber, Beijing, China), and Hoechst  
118 33342/PI Double Staining Kit (Solarbio). To minimize well-to-well variation and edge effects, cells  
119 were seeded in equal numbers under consistent experimental conditions. For the CCK-8 assay, cells  
120 were seeded into 96-well plates at a density of  $1 \times 10^4$  cells/well and treated with various  
121 concentrations (20, 40, 60, 80, and 100 µM) of ISO (HerbPurify Co., Chengdu, China) or 5-FU  
122 (MedChem Express, Princeton, USA) for different durations (6, 12, 18, 24, and 30 hours (h)). After  
123 treatment, 10 µl of CCK-8 solution was added to each well, followed by incubation for an  
124 additional 3 h. Absorbance was measured at 490 nm using a microplate reader (Tecan, Shanghai,  
125 China) to evaluate cell viability in both carcinoma and normal cell lines.

126 For the Trypan Blue exclusion assay, Huh-7 cells ( $1 \times 10^5$  cells/well) were seeded in 6 cm dishes  
127 and treated with 43 µM 5-FU or 27 µM ISO (IC<sub>50</sub> value) for various time intervals (3, 6, 12, and 24  
128 h). Cells were stained with 0.4% Trypan Blue for 3 minutes (min), and morphological changes were  
129 observed under a fluorescence microscope (MSHOT, Guangzhou, China).

130 For the Hoechst 33342/PI double staining assay, cells were cultured and treated identically to the  
131 Trypan Blue assay. Cells were then stained with Hoechst 33342 and propidium iodide (PI) for 20  
132 min according to the manufacturer's instructions, and fluorescence intensity was measured.

133 **Network pharmacology analysis and molecular docking analysis.** Network pharmacology is a  
134 bioinformatics-based approach that integrates multiple omics data to predict drug-target interactions  
135 and elucidate underlying mechanisms. In this study, we performed an integrated network  
136 pharmacology analysis combined with molecular docking validation to systematically investigate  
137 the antitumor mechanism of ISO in HCC. The overall workflow is illustrated in Supplementary  
138 Figure S1.

139 Liver cancer-associated target genes were collected via the GeneCards database  
140 (<https://www.genecards.org/>, accessed on 20 July 2024) using the keyword “hepatocellular  
141 carcinoma” and filtering for genes with a relevance score above the median value. The standard  
142 linear chemical structure of ISO was obtained from the PubChem database  
143 (<https://pubchem.ncbi.nlm.nih.gov/>, accessed on 20 July 2024), and its 2D and 3D structures were  
144 downloaded. Potential ISO-related targets were predicted using the Swiss Target Prediction  
145 database (<http://www.swisstargetprediction.ch/>, accessed on 20 July 2024) with a probability score  
146 cutoff  $> 0.7$  and supplemented by literature review. Only human entries were retained, and  
147 redundant records were merged.

148 The Venny 2.1.0 tool (<https://bioinfo.gp.cnb.csic.es/tools/venny/>, accessed on 20 July 2024) was  
149 used to identify overlapping targets between ISO and HCC. The PPI network was constructed with  
150 the following parameters: organism “Homo sapiens,” a minimum required interaction score of 0.4,  
151 and hiding disconnected nodes in the network. Overlapping genes were submitted to the STRING  
152 database (Version 11.0; <http://www.string-db.org/>, accessed on 20 July 2024), and network  
153 visualization and refinement were performed using Cytoscape software (version 3.7.2;  
154 <https://cytoscape.org/>, accessed on 20 July 2024). GO enrichment analysis was carried out using the  
155 DAVID platform (<https://davidbioinformatics.nih.gov/>, accessed on 20 July 2024), along with  
156 KEGG pathway enrichment analysis. GO and KEGG enrichment analysis were considered  
157 significantly enriched at  $p < 0.05$ . These analyses revealed key signaling pathways potentially  
158 involved in the antitumor effects of ISO.

159 To validate the binding feasibility between ISO and the key targets predicted by the network  
160 pharmacology analysis, molecular docking was performed. The core compound ISO was used as  
161 the small-molecule ligand, and the core targets from the PPI network were selected as docking  
162 receptors. The two-dimensional SDF structure of ISO was downloaded from the PubChem database,  
163 and the PDB-format structures of key target proteins were obtained from the RCSB Protein Data  
164 Bank (<https://www.rcsb.org/>, accessed on 20 July 2024). In PyMOL software, water molecules were  
165 removed from the target proteins, and ligand preparation was conducted. Using AutoDockTools  
166 1.5.7, the target proteins were hydrogenated, charges were assigned, and atomic rigid structures  
167 were determined. Docking grids were generated to define active binding pockets, and molecular  
168 docking was performed using the built-in docking tool. Binding affinities were estimated as free

169 energy of binding (kcal/mol); lower values indicate stronger interactions. The molecular docking  
170 results were visualized using PyMOL software.

171 **Cell apoptosis analysis.** Apoptosis was analyzed using an Annexin V-FITC/PI apoptosis detection  
172 kit (4A Biotech, Beijing, China). The cell culture and treatment conditions were consistent with  
173 those used in the Hoechst/PI double staining assay. Briefly, 200  $\mu$ l of  $1\times$  binding buffer and 4  $\mu$ l of  
174 Annexin V-FITC were added to each sample. The cells were incubated in the dark at room  
175 temperature for 5 min. Following this, 3  $\mu$ l of PI was added, and the samples were incubated at 4  $^{\circ}$ C  
176 for 20 min. Apoptotic morphological changes and staining were observed by fluorescence  
177 microscopy. In addition, the percentage of apoptotic cells was quantified using flow cytometry  
178 (Sysmex Co., Kobe, Japan).

179 **Mitochondrial membrane potential analysis.** MMP was assessed using the JC-1 MMP assay kit  
180 (Solarbio). Huh-7 cells ( $1 \times 10^5$  cells/well) were seeded in 6 cm culture dishes and treated with 43  
181  $\mu$ M 5-FU or 27  $\mu$ M ISO at various time points (3, 6, 12, and 24 h). After treatment, 1 ml of  $1\times$  JC-1  
182 staining solution was added to each well, followed by a 30 min incubation. Cells were then  
183 centrifuged for 3 min, washed twice with  $1\times$  washing buffer, and subjected to flow cytometry for  
184 MMP analysis. The effect of ISO on MMP in Huh-7 cells was recorded.

185 **Western blotting analysis.** Western blotting was conducted to assess protein expression associated  
186 with apoptosis and related pathways. Huh-7 cells ( $1 \times 10^5$  cells/well) were cultured in 6 cm dishes  
187 and treated with 27  $\mu$ M ISO for 3, 6, 12, or 24 h. A total of 2 ml of lysis buffer was added to each  
188 sample based on cell density. Distilled deionized water (DDW) and  $5\times$  sample buffer was added  
189 according to optical density (OD) values. Equal amounts of protein (20  $\mu$ g/sample) were loaded  
190 onto SDS-PAGE gels. After electrophoresis and transfer, membranes were incubated with specific  
191 antibodies against phosphorylated ERK (p-ERK, #sc-7383), ERK (#sc-154), phosphorylated JNK  
192 (p-JNK, #sc-6254), JNK (#sc-7345), phosphorylated p38 (p-p38, #sc-7973), p38 (#sc-7149),  
193 phosphorylated AKT (p-AKT, #sc-7985-R), AKT (#sc-8312), phosphorylated STAT3 (p-STAT3,  
194 #sc-8059), STAT3 (#sc-8019), Bad (#sc-8044), Bcl-2 (#sc-7382), cytochrome c (cyto-c, #sc-13156),  
195 cleaved-caspase-3 (cle-casp-3, #sc-271028), cleaved-PARP (cle-PARP, #sc-8007), Cyclin B1  
196 (#sc-245), CDK1/2 (#sc-53219), p21 (#sc-397), p27 (#sc-528), phosphorylated GSK-3 $\beta$  (p-GSK-3 $\beta$ ,  
197 #sc-16740-R), GSK-3 $\beta$  (#sc-7291),  $\beta$ -catenin (#sc-7963), E-cadherin (#sc-8426), and N-cadherin  
198 (#sc-59987) and  $\alpha$ -tubulin (#sc-69971). All aforementioned antibodies were purchased from Santa

199 Cruz Biotechnology (Dallas, TX, USA). Secondary antibodies, including horseradish peroxidase  
200 (HRP)-conjugated goat anti-rabbit IgG and goat anti-mouse IgG, were obtained from ZSGB-Bio  
201 (Beijing, China).

202 **Cell ROS analysis.** ROS levels were analyzed using an ROS detection kit (Solarbio). Huh-7 cells  
203 ( $1 \times 10^5$  cells/well) were cultured in 6 cm dishes and treated with 43  $\mu$ M 5-FU or 27  $\mu$ M ISO at  
204 multiple time points (3, 6, 12, and 24 h). Cells were incubated with 2',7'-dichlorodihydrofluorescein  
205 diacetate (DCFH-DA) in the dark for 30 min. ROS accumulation was subsequently measured by  
206 flow cytometry and fluorescence microscopy. For further validation, Huh-7 cells were pretreated  
207 with N-acetyl cysteine (NAC) for 30 min prior to ISO treatment, and ROS levels were re-evaluated.

208 **Cell cycle analysis.** Cell cycle analysis was conducted using the Ki67 Cell Proliferation Assay Kit  
209 (Beyotime, Shanghai, China) and the DNA Content Quantitative Assay Kit (Solarbio, Beijing,  
210 China). Huh-7 cells ( $1 \times 10^5$  cells/well) were seeded onto 6 cm culture plates. Subsequently, these  
211 cells were treated with 43  $\mu$ M 5-FU and 27  $\mu$ M ISO at multiple predetermined time intervals (3, 6,  
212 12, and 24 h). Cells in each well were fixed with 1 ml of fixative for 5 min, followed by the addition  
213 of 1 ml of immunostaining blocking solution. After 10 min, 1 ml of Ki67 rabbit monoclonal  
214 antibody was added and the samples were incubated overnight at 4 °C. Following three washes with  
215 washing solution, 1 ml of anti-rabbit 488 secondary antibody was added and incubated at room  
216 temperature for 1 h. Next, 1 ml of nuclear staining solution (DAPI) was added to each well for 5  
217 min. After an additional three washes, the effects of 5-FU and ISO on cell cycle arrest in Huh-7  
218 cells were visualized using fluorescence microscopy.

219 The cell culture and treatment procedures for DNA content analysis were consistent with the  
220 Ki67/PI double staining method. Cells were subsequently fixed in 70% ethanol and stored at 4 °C  
221 overnight. The next day, cells were incubated with 100  $\mu$ L of RNase A at 37 °C for 30 min.  
222 Following this, 400  $\mu$ l of PI was added, and the samples were incubated in the dark at 4 °C for  
223 another 30 min. Flow cytometry was then used to evaluate the effects of 5-FU and ISO on cell cycle  
224 arrest in Huh-7 cells. Data were subsequently analyzed using Flow Jo 10.8 software. Prior to ISO  
225 treatment, Huh-7 cells were pretreated for 30 min with NAC and the AKT inhibitor HY10249, then  
226 reanalyzed.

227 **Cell migration analysis.** Cell migration was assessed using the wound healing assay. Huh-7 cells  
228 ( $1 \times 10^5$  cells/well) were seeded onto 6 cm culture plates and treated with 43  $\mu$ M 5-FU and 27  $\mu$ M

229 ISO at multiple predetermined time intervals (3, 6, 12, and 24 h). For the Transwell assay, Huh-7  
230 cells at a density of  $1 \times 10^5$ /ml were seeded into the upper chamber of a Transwell insert. The lower  
231 chamber was filled with medium containing 20% FBS and incubated for 24 h. The cells were then  
232 treated with 43  $\mu$ M 5-FU and 27  $\mu$ M ISO at various time points (3, 6, 12, and 24 h). After  
233 incubation, cells were stained using 0.1% crystal violet. Migrated cells were quantified using the  
234 Transwell assay and visualized by fluorescence microscopy.

235 In additional experiments, Huh-7 cells were pretreated with 10 mM NAC for 30 min, or with both  
236 10 mM NAC and the AKT inhibitor HY10249 for 30 min prior to ISO treatment, and migration was  
237 reassessed.

238 **Statistical analysis.** All experiments were conducted in triplicate, and the results were expressed as  
239 mean $\pm$ standard deviation (SD). IC<sub>50</sub> values were calculated using GraphPad Prism 10.0. One-way  
240 analysis of variance (ANOVA) was performed using SPSS 21.0, and statistical significance was  
241 determined using T-tests. Significance thresholds were set as follows: \*p < 0.05, \*\*p < 0.01, and  
242 \*\*\*p < 0.001.

243

## 244 **Results**

245 **Cytotoxic effects of ISO.** ISO exhibited a potent cytotoxic effect on three HCC cell lines: Huh-7,  
246 HepG2, and Hep3B. The cytotoxicity of ISO displayed both concentration and time-dependent  
247 effects on liver cancer cell viability (Figures 1A, 1B). In contrast, the toxicity of ISO toward four  
248 normal human cell lines-THLE-2, IMR-90, 293T, and GES-1 was significantly lower than that  
249 observed for 5-fluorouracil (5-FU) (Figures 1C, 1D). The half-maximal inhibitory concentration  
250 (IC<sub>50</sub>) values for Huh-7, HepG2, and Hep3B cells treated with ISO were 27  $\mu$ M, 80  $\mu$ M, and 62  $\mu$ M,  
251 respectively. Compared with 5-FU, an increase in the duration of ISO treatment led to a progressive  
252 increase in the number of Trypan blue-stained cells (Figure 1E). Additionally, the proportion of  
253 Huh-7 cells with both bright Hoechst 33342 and PI fluorescence was increased with prolonged ISO  
254 treatment. (Figure 1F). These findings suggest that ISO exerts superior cytotoxicity against Huh-7  
255 cells compared to 5-FU. Consequently, Huh-7 cells were selected as the target model for subsequent  
256 experiments.

257 **ISO and HCC network pharmacology.** To prepare for the subsequent target prediction, we  
258 visualized the chemical structure of ISO (Figure 2A). Using SwissTargetPrediction (probability >

259 0.7, human), we identified 157 potential targets of ISO. From GeneCards (keyword: “hepatocellular  
260 carcinoma”), 2349 HCC-related targets were retrieved based on relevance score  $\geq$  median. Venny  
261 analysis revealed 110 overlapping targets (Figure 2B). Protein-protein interaction (PPI) networks  
262 were constructed using the STRING database and analyzed using Cytoscape software (Figures 2C,  
263 2D). Gene Ontology (GO) analysis indicated that these overlapping targets were mainly associated  
264 with the regulation of apoptosis, cell migration, and protein phosphorylation. Kyoto Encyclopedia  
265 of Genes and Genomes (KEGG) pathway analysis showed significant enrichment in cancer-related  
266 pathways, particularly those involving AKT, MAPK, and ROS signaling (Figures 2E-2G).

267 **ISO and HCC molecular docking analysis.** To predict the binding sites through which ISO  
268 interacts with liver cancer targets, a molecular docking analysis was performed. A comprehensive  
269 binding site map of ISO was generated using AutoDock Tools 1.5.7. AKT1, CASP3, and GSK3B  
270 were selected as the core protein receptors for docking simulations. The active docking pocket was  
271 set, and ISO formed hydrogen bonds with AKT1, CASP3, and GSK3B, indicating favorable  
272 docking conformations. Molecular docking models of ISO bound to AKT1, CASP3, and GSK3B  
273 were obtained from the PDB database (Figure 2H). The binding interfaces between ISO and AKT1  
274 or GSK3B included residues such as LEU, which may influence phosphorylation activity. These  
275 results suggest that ISO exhibits strong binding affinity toward AKT1, CASP3, and GSK3B.

276 **ISO induces mitochondria-mediated apoptosis in Huh-7 cells.** With prolonged ISO treatment,  
277 Huh-7 cells exhibited gradual shrinkage and nuclear fragmentation, and the proportion of apoptotic  
278 cells was increased. These morphological changes were more significant than those in the  
279 5-FU-treated group. (Figure 3A). Flow cytometry analysis revealed that ISO increased the  
280 proportion of apoptotic cells from 0.02% to 21.55%, while simultaneously reducing mitochondrial  
281 membrane potential (MMP) from 99.48% to 77.8% (Figures 3B, 3C). Western blotting results  
282 demonstrated that with prolonged ISO treatment, the expression levels of pro-apoptotic proteins  
283 including Bad, cytochrome c (cyto-c), cleaved caspase-3 (cle-casp-3), and cleaved PARP (cle-PARP)  
284 progressively increased. In contrast, the anti-apoptotic protein Bcl-2 exhibited reduced expression  
285 (Figure 3D). These findings indicate that ISO induces mitochondria-dependent apoptosis in Huh-7  
286 cells.

287 **ISO regulates MAPK/STAT3 signaling pathways in Huh-7 cells.** With increasing ISO treatment  
288 time, the expression levels of phosphorylated JNK (p-JNK) and phosphorylated p38 (p-p38)

289 increased, while the levels of phosphorylated ERK (p-ERK) and phosphorylated STAT3 (p-STAT3)  
290 decreased (Figure 3E). To investigate the interaction between MAPK and STAT3 signaling  
291 pathways, MAPK inhibitors were applied to Huh-7 cells. ERK inhibition led to decreased p-STAT3  
292 expression, whereas JNK and p38 inhibitors altered these effects (Figures 3F-3H). These results  
293 suggest that the MAPK pathway promotes apoptosis in Huh-7 cells through modulation of the  
294 STAT3 signaling pathway.

295 **ISO upregulates ROS levels via MAPK/STAT3 signaling pathways in Huh-7 cells.** ISO  
296 treatment led to a progressive increase in ROS accumulation within Huh-7 cells. Compared with  
297 5-FU, ISO induced a greater increase in ROS fluorescence intensity over time (Figures 4A-4C). In  
298 the ISO+NAC group, fluorescence intensity was considerably reduced relative to ISO treatment  
299 alone, indicating effective ROS scavenging by NAC. Pretreatment with NAC for 30 min  
300 significantly reduced the number of apoptotic Huh-7 cells (Figure 4D). Furthermore, the expression  
301 levels of p-ERK, p-JNK, p-p38, p-STAT3, cle-casp-3, and cle-PARP were inhibited in the  
302 ISO+NAC group compared with ISO treatment alone (Figure 4E). These results collectively  
303 demonstrate that ISO elevates intracellular ROS levels, which in turn mediate apoptosis through the  
304 MAPK signaling pathway in Huh-7 cells.

305 **ISO Triggers G2/M cell cycle arrest in Huh-7 cells.** As ISO treatment duration increased, the  
306 fluorescence intensity of Huh-7 cells stained with Ki67 decreased, indicating suppressed  
307 proliferation. The effect was comparable to that of 5-FU (Figure 5A). Flow cytometry results  
308 showed that ISO treatment significantly elevated the proportion of Huh-7 cells in the G2/M phase  
309 from 11.7% to 34.9%, while the percentage of cells in the G0/G1 phase progressively declined  
310 (Figure 5B). When comparing the ISO+NAC group with ISO treatment alone, the ISO-induced  
311 G2/M phase arrest increased from 16.8% to 27.3% (Figure 5C). Western blotting analysis revealed  
312 that ISO significantly downregulated the expression of p-AKT, CDK1/2, and Cyclin B, while  
313 upregulating p21 and p27 levels in Huh-7 cells. Following pretreatment with NAC or the AKT  
314 inhibitor HY10249, marked changes in cell cycle-related protein expression were also observed  
315 relative to the inhibitor-only groups (Figures 5C, 5D). These findings demonstrate that ISO can  
316 induce G2/M phase cell cycle arrest in Huh-7 cells.

317 **ISO prevents Huh-7 cell migration via the AKT/GSK-3 $\beta$ / $\beta$ -catenin signaling pathways.**  
318 Inverted fluorescence microscopy revealed that ISO significantly inhibited Huh-7 cell migration

319 compared with 5-FU, with a time-dependent effect (Figures 6A-6D). Western blotting demonstrated  
320 increased expression of E-cadherin and reduced expression of p-AKT, p-GSK-3 $\beta$ , N-cadherin, and  
321  $\beta$ -catenin following ISO treatment. The addition of NAC or the AKT inhibitor HY10249 suppressed  
322 these protein expression changes (Figures 6E-6G). Collectively, these findings indicate that ISO  
323 impairs Huh-7 cell migration by regulating the AKT/GSK-3 $\beta$ / $\beta$ -catenin signaling pathways.

324

325

Accepted manuscript

326 **Discussion**

327 In recent years, the use of Chinese herbal medicine in tumor therapy has gained increasing attention  
328 due to its potential to inhibit tumor growth and induce apoptosis in cancer cells [31-34]. Croton, a  
329 traditional Chinese herb, has demonstrated therapeutic properties including antibacterial,  
330 anti-inflammatory, and antiproliferative effects, particularly in MDA-MB-231 breast cancer cells  
331 [35]. ISO, the focus of this study, is an important alkaloid component derived from croton [36].  
332 However, the precise molecular mechanisms underlying ISO's anticancer activity have not yet been  
333 fully elucidated. 5-FU is a widely used chemotherapeutic agent known to induce apoptosis in  
334 various cancer types [37]. Our results demonstrated that ISO significantly inhibited Huh-7 cell  
335 proliferation while exerting lower cytotoxicity on normal cells compared with 5-FU, suggesting that  
336 ISO may represent a more promising candidate for anticancer drug development. Notably, ISO was  
337 shown to induce G2/M cell cycle arrest, apoptosis, and inhibition of migration, primarily through  
338 the upregulation of intracellular ROS.

339 Apoptosis is a tightly regulated process triggered in response to external environmental stressors  
340 and involves complex molecular pathways [38, 39]. Members of the Bcl-2 protein family play a  
341 pivotal role in modulating mitochondrial membrane permeability [40, 41]. A decrease in MMP  
342 facilitates cyto-c release, activates caspase-3, and ultimately leads to programmed cell death [42-44].  
343 Previous studies on croton extracts have shown that they can activate caspase cascades and  
344 modulate pro- and anti-apoptotic gene expression to induce mitochondrial-mediated apoptosis [35].  
345 Consistent with these findings, our study demonstrated that ISO increased the expression of the  
346 pro-apoptotic protein Bad, decreased Bcl-2 expression, reduced MMP, and triggered apoptosis in  
347 Huh-7 cells.

348 To further elucidate the mechanisms underlying ISO-induced apoptosis, we employed network  
349 pharmacology. The analysis revealed enhanced protein phosphorylation activity, with protein kinase  
350 and serine/threonine/tyrosine kinase functions playing central roles in the biological processes.  
351 MAPK, a serine/threonine kinase, is critically involved in cancer cell apoptosis initiated by natural  
352 compounds [45, 46]. In our study, ISO significantly downregulated the expression levels of p-ERK  
353 and p-STAT3, further implicating these pathways in its pro-apoptotic effects.

354 ROS are key regulators of tumor biology, influencing tumor progression, signaling, and cell death  
355 [47]. Croton-derived compounds have previously been shown to elevate ROS levels in breast cancer

356 cells [35]. Consistent with this, our findings demonstrated that ISO induced a sustained increase in  
357 ROS levels in Huh-7 cells. To assess the role of ROS in ISO-induced apoptosis, NAC (a ROS  
358 scavenger) was used for pretreatment. NAC significantly reduced the proportion of apoptotic cells  
359 and altered the expression of key proteins in the AKT, MAPK, and STAT3 pathways. These  
360 observations suggest that ROS serve as upstream signals in ISO-induced activation of these  
361 pathways, promoting apoptosis through enhanced mitochondrial ROS production. Collectively,  
362 these findings indicate that ISO is a promising candidate for development as a novel antitumor  
363 agent.

364 Cell cycle regulation plays a fundamental role in controlling cell proliferation and apoptosis, and is  
365 critically involved in tumor initiation and progression [48]. Due to significant variability across cell  
366 cycle phases, precise control of cell cycle dynamics remains challenging [49]. Recent studies have  
367 shown that various anticancer agents can induce cell cycle arrest and stabilize cell cycle checkpoints  
368 [50, 51]. The natural product B10G5 derived from *Croton tiglium* has been reported to induce  
369 G2/M phase arrest and initiate apoptosis in lung cancer cells [52]. In our study, ISO was found to  
370 induce G2/M phase arrest in Huh-7 cells by downregulating AKT expression, leading to decreased  
371 levels of p-AKT, CDK1/2, and Cyclin B1, and increased levels of p27 and p21. These changes  
372 effectively contributed to the suppression of tumorigenic potential.

373 Cell migration is essential for maintaining tissue organization [53].  $\beta$ -catenin is a well-known  
374 substrate of GSK-3 $\beta$ , and its phosphorylation is modulated by GSK-3 $\beta$  activity [54].  
375 Overexpression or activation of GSK-3 $\beta$  can promote AKT phosphorylation, which is implicated in  
376 tumor progression and cell motility [55]. Our results showed that ISO decreased the expression of  
377 N-cadherin, increased E-cadherin levels, and inhibited Huh-7 cell migration. Moreover, NAC  
378 pretreatment abrogated these effects by suppressing ROS accumulation and its downstream  
379 influence on migration-associated proteins. These findings suggest that ISO impairs Huh-7 cell  
380 migration through ROS-induced modulation of the AKT/GSK-3 $\beta$ / $\beta$ -catenin signaling pathway.

381 The strength of this study lies in the integration of network pharmacology, molecular docking, and  
382 experimental validation to systematically elucidate the antitumor mechanism of ISO in HCC. This  
383 multidisciplinary approach not only identified key signaling pathways (e.g., AKT, MAPK, STAT3)  
384 but also linked them to functional phenotypes such as apoptosis, cell cycle arrest, and migration  
385 inhibition, providing a comprehensive mechanistic framework. The convergence of computational

386 prediction and in vitro validation enhances the reliability and translational potential of the findings.  
387 However, this study has certain limitations that should be acknowledged. The absence of in vivo  
388 animal model data limits the translation of our cellular findings to a whole-organism context. Future  
389 studies employing orthotopic or xenograft mouse models are essential to confirm the antitumor  
390 efficacy and safety profile of ISO in vivo. Beyond conventional cytotoxicity, exploring ISO within  
391 the context of drug repurposing and sustainable therapeutic strategies could be highly valuable.  
392 Specifically, repurposing drugs as GLP-1-based therapies or targeting 20S proteasomes as a  
393 prophylactic strategy with immunomodulatory effects has shown positive impacts on cancer  
394 management [56, 57]. Future work could investigate whether ISO or its derivatives share  
395 mechanistic similarities with these approaches, potentially positioning it within a broader  
396 framework for cancer prevention or combination therapy. We believe that addressing these  
397 limitations in future research will help fully exploit the potential of ISO as a novel therapeutic agent  
398 for HCC.

399 In summary, ISO induces apoptosis in Huh-7 cells through ROS accumulation, which activates the  
400 MAPK/STAT3 signaling pathways and modulates downstream apoptotic proteins. Simultaneously,  
401 ISO inhibits the AKT signaling pathway to induce G2/M phase cell cycle arrest and suppresses cell  
402 migration via ROS-mediated regulation of the GSK-3 $\beta$ / $\beta$ -catenin axis. These findings (Figure 7)  
403 provide a theoretical basis for further pharmacological research and support the potential  
404 development and application of ISO as an anticancer agent.

405  
406 Acknowledgements: We thank LetPub ([www.letpub.com](http://www.letpub.com)) for their linguistic assistance during the  
407 preparation of this manuscript.

408 This research was funded by, the National Natural Science Foundation of China (Grant No.  
409 82460126), the Program for Young Talents of Science and Technology in Universities of Inner  
410 Mongolia Autonomous Region (Grant No. NJYT24032), and the Heilongjiang Province Key  
411 Re-search and Development Plan Guidance Project (Grant No. GZ20220039).

412  
413 **Supplementary data are available in the online version of the paper.**

414

415

416 **References**

- 417 [1] LLOVET JM, ZUCMAN-ROSSI J, PIKARSKY E, SANGRO B, SCHWARTZ M et al.  
418 Hepatocellular carcinoma. *Nat Rev Dis Primers* 2016; 2: 16018.  
419 <https://doi.org/10.1038/nrdp.2016.18>
- 420 [2] FORNER A, REIG M, BRUIX J. Hepatocellular carcinoma. *Lancet* 2018; 391: 1301-1314.  
421 [https://doi.org/10.1016/s0140-6736\(18\)30010-2](https://doi.org/10.1016/s0140-6736(18)30010-2)
- 422 [3] FOGLIA B, TURATO C, CANNITO S. Hepatocellular Carcinoma: Latest Research in  
423 Pathogenesis, Detection and Treatment. *Int J Mol Sci* 2023; 24: 12224.  
424 <https://doi.org/10.3390/ijms241512224>
- 425 [4] YOUNESS RA, HASSAN HA, ABAZA T, HADY AA, EL MAGDOUB HM et al. A  
426 Comprehensive Insight and In Silico Analysis of CircRNAs in Hepatocellular Carcinoma: A  
427 Step toward ncRNA-Based Precision Medicine. *Cells* 2024; 13: 1245.  
428 <https://doi.org/10.3390/cells13151245>
- 429 [5] SIM HW, KNOX J. Hepatocellular carcinoma in the era of immunotherapy. *Curr Probl*  
430 *Cancer* 2018; 42: 40-48. <https://doi.org/10.1016/j.currprobcancer.2017.10.007>
- 431 [6] NYGREN P. What is cancer chemotherapy? *Acta Oncol* 2001; 40: 166-174.  
432 <https://doi.org/10.1080/02841860151116204>
- 433 [7] WIEMANN MC, CALABRESI P. Principles of current cancer chemotherapy. *Compr Ther*  
434 1983; 9: 46-52.
- 435 [8] CHEN LC, LIN HY, HUNG SK, CHIOU WY, LEE MS. Role of modern radiotherapy in  
436 managing patients with hepatocellular carcinoma. *World J Gastroenterol* 2021; 27:  
437 2434-2457. <https://doi.org/10.3748/wjg.v27.i20.2434>
- 438 [9] ORONSKY B, SCICINSKI J, KIM MM, CABRALES P, SALACZ ME et al. Turning on the  
439 Radio: Epigenetic Inhibitors as Potential Radiopriming Agents. *Biomolecules* 2016; 6: 32.  
440 <https://doi.org/10.3390/biom6030032>
- 441 [10] WANG C, SHI CH, BAI HY, LU J, HU HT et al. Astragali radix - Curcumae rhizoma herb  
442 pair suppresses hepatocellular carcinoma through EGFR/AKT/mTOR pathway and induces  
443 lipid peroxidation-related ferroptosis via HIF-1 $\alpha$ /HO-1/GPX4 axis. *J Ethnopharmacol* 2025;  
444 348: 119912. <https://doi.org/10.1016/j.jep.2025.119912>
- 445 [11] ZHONG M, LI Y, WANG H, FAN N, CHU X et al. Integrated network pharmacology and  
446 experimental validation reveal EGFR/p53/Bcl-2-mediated anti-hepatocellular carcinoma  
447 effects of Zedoary Turmeric Oil. *J Ethnopharmacol* 2025; 352: 120241.  
448 <https://doi.org/10.1016/j.jep.2025.120241>
- 449 [12] ZHAI B, ZHANG N, HAN X, LI Q, ZHANG M et al. Molecular targets of  $\beta$ -elemene, a  
450 herbal extract used in traditional Chinese medicine, and its potential role in cancer therapy:  
451 A review. *Biomed Pharmacother* 2019; 114: 108812.  
452 <https://doi.org/10.1016/j.biopha.2019.108812>
- 453 [13] DING T, TANG F, NI G, LIU J, ZHAO H et al. The development of isoguanosine: from  
454 discovery, synthesis, and modification to supramolecular structures and potential  
455 applications. *RSC Adv* 2020, 10: 6223-6248. <https://doi.org/10.1039/C9RA09427J>
- 456 [14] KIM JH, LEE SJ, HAN YB, MOON JJ, KIM JB. Isolation of isoguanosine from *Croton*  
457 *tiglium* and its antitumor activity. *Arch Pharm Res* 1994; 17: 115-118.  
458 <https://doi.org/10.1007/bf02974234>

- 459 [15] ZHAO H, FENG H, LIU J, TANG F, DU Y et al. Dual-functional guanosine-based hydrogel  
460 integrating localized delivery and anticancer activities for cancer therapy. *Biomaterials*  
461 2020; 230: 119598. <https://doi.org/10.1016/j.biomaterials.2019.119598>
- 462 [16] YU L, HUANG K, LIAO Y, WANG L, SETHI G et al. Targeting novel regulated cell death:  
463 Ferroptosis, pyroptosis and necroptosis in anti-PD-1/PD-L1 cancer immunotherapy. *Cell*  
464 *Prolif* 2024; 57: e13644. <https://doi.org/10.1111/cpr.13644>
- 465 [17] LI R, WU Y, LI Y, SHUAI W, WANG A et al. Targeted regulated cell death with small  
466 molecule compounds in colorectal cancer: Current perspectives of targeted therapy and  
467 molecular mechanisms. *Eur J Med Chem* 2024; 265: 116040.  
468 <https://doi.org/10.1016/j.ejmech.2023.116040>
- 469 [18] QIN R, YOU FM, ZHAO Q, XIE X, PENG C et al. Naturally derived indole alkaloids  
470 targeting regulated cell death (RCD) for cancer therapy: from molecular mechanisms to  
471 potential therapeutic targets. *J Hematol Oncol* 2022; 15: 133.  
472 <https://doi.org/10.1186/s13045-022-01350-z>
- 473 [19] KIM C, KIM B. Anti-Cancer Natural Products and Their Bioactive Compounds Inducing ER  
474 Stress-Mediated Apoptosis: A Review. *Nutrients* 2018; 10: 1021.  
475 <https://doi.org/10.3390/nu10081021>
- 476 [20] TONG X, TANG R, XIAO M, XU J, WANG W et al. Targeting cell death pathways for  
477 cancer therapy: recent developments in necroptosis, pyroptosis, ferroptosis, and cuproptosis  
478 research. *J Hematol Oncol* 2022; 15: 174. <https://doi.org/10.1186/s13045-022-01392-3>
- 479 [21] XU X, LAI Y, HUA ZC. Apoptosis and apoptotic body: disease message and therapeutic  
480 target potentials. *Biosci Rep* 2019; 39: BSR20180992. <https://doi.org/10.1042/bsr20180992>
- 481 [22] JEONG SY, SEOL DW. The role of mitochondria in apoptosis. *BMB Rep* 2008; 41: 11-22.  
482 <https://doi.org/10.5483/bmbrep.2008.41.1.011>
- 483 [23] WANG H, ZHANG C, LI M, LIU C, WANG J et al. Antimicrobial Peptides Mediate  
484 Apoptosis by Changing Mitochondrial Membrane Permeability. *Int J Mol Sci* 2022; 23:  
485 12732. <https://doi.org/10.3390/ijms232112732>
- 486 [24] SAHOO BM, BANIK BK, BORAH P, JAIN A. Reactive Oxygen Species (ROS): Key  
487 Components in Cancer Therapies. *Anticancer Agents Med Chem* 2022; 22: 215-222.  
488 <https://doi.org/10.2174/1871520621666210608095512>
- 489 [25] BRIEGER K, SCHIAVONE S, MILLER FJ JR, KRAUSE KH. Reactive oxygen species:  
490 from health to disease. *Swiss Med Wkly* 2012; 142: w13659.  
491 <https://doi.org/10.4414/smw.2012.13659>
- 492 [26] PAN Z, WANG K, WANG X, JIA Z, YANG Y et al. Cholesterol promotes EGFR-TKIs  
493 resistance in NSCLC by inducing EGFR/Src/Erk/SP1 signaling-mediated ERR $\alpha$   
494 re-expression. *Mol Cancer* 2022; 21: 77. <https://doi.org/10.1186/s12943-022-01547-3>
- 495 [27] CHEN Z, OH D, DUBEY AK, YAO M, YANG B et al. EGFR family and Src family kinase  
496 interactions: mechanics matters? *Curr Opin Cell Biol* 2018; 51: 97-102.  
497 <https://doi.org/10.1016/j.ceb.2017.12.003>
- 498 [28] TICE DA, BISCARDI JS, NICKLES AL, PARSONS SJ. Mechanism of biological synergy  
499 between cellular Src and epidermal growth factor receptor. *Proc Natl Acad Sci U S A* 1999;  
500 96: 1415-1420. <https://doi.org/10.1073/pnas.96.4.1415>
- 501 [29] BASU A, DAS AS, BORAH PK, DUARY RK, MUKHOPADHYAY R. Biochanin A  
502 impedes STAT3 activation by upregulating p38 $\delta$  MAPK phosphorylation in IL-6-stimulated

- 503 macrophages. *Inflamm Res* 2020; 69: 1143-1156.  
 504 <https://doi.org/10.1007/s00011-020-01387-1>
- 505 [30] MENG A, ZHANG X, SHI Y. Role of p38 MAPK and STAT3 in  
 506 lipopolysaccharide-stimulated mouse alveolar macrophages. *Exp Ther Med* 2014; 8:  
 507 1772-1776. <https://doi.org/10.3892/etm.2014.2023>
- 508 [31] DAI XZ, YIN HT, SUN LF, HU X, ZHOU C et al. Potential therapeutic efficacy of  
 509 curcumin in liver cancer. *Asian Pac J Cancer Prev* 2013; 14: 3855-3859.  
 510 <https://doi.org/10.7314/apjcp.2013.14.6.3855>
- 511 [32] LUO H, VONG CT, CHEN H, GAO Y, LYU P et al. Naturally occurring anti-cancer  
 512 compounds: shining from Chinese herbal medicine. *Chin Med* 2019; 14: 48.  
 513 <https://doi.org/10.1186/s13020-019-0270-9>
- 514 [33] YAN Z, LAI Z, LIN J. Anticancer Properties of Traditional Chinese Medicine. *Comb Chem*  
 515 *High Throughput Screen* 2017; 20: 423-429.  
 516 <https://doi.org/10.2174/1386207320666170116141818>
- 517 [34] ZHANG X, QIU H, LI C, CAI P, QI F. The positive role of traditional Chinese medicine as  
 518 an adjunctive therapy for cancer. *Biosci Trends* 2021; 15: 283-298.  
 519 <https://doi.org/10.5582/bst.2021.01318>
- 520 [35] POOFERY J, SRIPANIDKULCHAI B, BANJERDPONGCHAI R. Extracts of *Bridelia*  
 521 *ovata* and *Croton oblongifolius* induce apoptosis in human MDA- MB- 231 breast cancer  
 522 cells via oxidative stress and mitochondrial pathways. *Int J Oncol* 2020; 56: 969-985.  
 523 <https://doi.org/10.3892/ijo.2020.4973>
- 524 [36] YAN P, ZHANG L, PENG C, ZHANG R. Pharmacokinetics and tissue distribution of  
 525 crotonoside. *Xenobiotica* 2018; 48: 28-36. <https://doi.org/10.1080/00498254.2016.1276311>
- 526 [37] LACOURSE KD, ZEPEDA-RIVERA M, KEMPCHINSKY AG, BARYIAMES A, MINOT  
 527 SS et al. The cancer chemotherapeutic 5-fluorouracil is a potent *Fusobacterium nucleatum*  
 528 inhibitor and its activity is modified by intratumoral microbiota. *Cell Rep* 2022; 41: 111625.  
 529 <https://doi.org/10.1016/j.celrep.2022.111625>
- 530 [38] KASHYAP D, GARG VK, GOEL N. Intrinsic and extrinsic pathways of apoptosis: Role in  
 531 cancer development and prognosis. *Adv Protein Chem Struct Biol* 2021; 125: 73-120.  
 532 <https://doi.org/10.1016/bs.apcsb.2021.01.003>
- 533 [39] D'ARCY MS. Cell death: a review of the major forms of apoptosis, necrosis and autophagy.  
 534 *Cell Biol Int* 2019; 43: 582-592. <https://doi.org/10.1002/cbin.11137>
- 535 [40] KLUCK RM, BOSSY-WETZEL E, GREEN DR, NEWMAYER DD. The release of  
 536 cytochrome c from mitochondria: a primary site for Bcl-2 regulation of apoptosis. *Science*  
 537 1997; 275: 1132-1136. <https://doi.org/10.1126/science.275.5303.1132>
- 538 [41] HARRIS MH, THOMPSON CB. The role of the Bcl-2 family in the regulation of outer  
 539 mitochondrial membrane permeability. *Cell Death Differ* 2000; 7: 1182-1191.  
 540 <https://doi.org/10.1038/sj.cdd.4400781>
- 541 [42] CHONG SJ, LOW IC, PERVAIZ S. Mitochondrial ROS and involvement of Bcl-2 as a  
 542 mitochondrial ROS regulator. *Mitochondrion* 2014; 19: 39-48.  
 543 <https://doi.org/10.1016/j.mito.2014.06.002>
- 544 [43] ITO T. [Overexpression of bcl-2 suppresses apoptosis in the human leukemia cell line TF-1]  
 545 *Rinsho Byori* 1997; 45: 628-637.

- 546 [44] KALONI D, DIEPSTRATEN ST, STRASSER A, KELLY GL. BCL-2 protein family:  
547 attractive targets for cancer therapy. *Apoptosis* 2023; 28: 20-38.  
548 <https://doi.org/10.1007/s10495-022-01780-7>
- 549 [45] FANG JY, RICHARDSON BC. The MAPK signalling pathways and colorectal cancer.  
550 *Lancet Oncol* 2005; 6: 322-327. [https://doi.org/10.1016/s1470-2045\(05\)70168-6](https://doi.org/10.1016/s1470-2045(05)70168-6)
- 551 [46] ASL ER, AMINI M, NAJAFI S, MANSOORI B, MOKHTARZADEH A et al. Interplay  
552 between MAPK/ERK signaling pathway and MicroRNAs: A crucial mechanism regulating  
553 cancer cell metabolism and tumor progression. *Life Sci* 2021; 278: 119499.
- 554 [47] MOLONEY JN, COTTER TG. ROS signalling in the biology of cancer. *Semin Cell Dev*  
555 *Biol* 2018; 80: 50-64. <https://doi.org/10.1016/j.semcdb.2017.05.023>
- 556 [48] SUN Y, LIU Y, MA X, HU H. The Influence of Cell Cycle Regulation on Chemotherapy. *Int*  
557 *J Mol Sci* 2021; 22. <https://doi.org/10.3390/ijms22136923>
- 558 [49] ONG G, LIU J, TANG X, ZHONG J, ZENG Y et al. Cell cycle checkpoint revolution:  
559 targeted therapies in the fight against malignant tumors. *Front Pharmacol* 2024; 15:  
560 1459057. <https://doi.org/10.3389/fphar.2024.1459057>
- 561 [50] LIU Y, WANG Y, YANG Y, QUAN Y, GUO M. Liquiritigenin Induces Cell Cycle Arrest and  
562 Apoptosis in Lung Squamous Cell Carcinoma. *Cell Biochem Biophys* 2024; 82: 1397-1407.  
563 <https://doi.org/10.1007/s12013-024-01294-w>
- 564 [51] LIU J, LI SM, TANG YJ, CAO JL, HOU WS et al. Jaceosidin induces apoptosis and inhibits  
565 migration in AGS gastric cancer cells by regulating ROS-mediated signaling pathways.  
566 *Redox Rep* 2024; 29: 2313366. <https://doi.org/10.1080/13510002.2024.2313366>
- 567 [52] WANG Y, TANG C, YAO S, LAI H, LI R et al. Discovery of a novel protein kinase C  
568 activator from *Croton tiglium* for inhibition of non-small cell lung cancer. *Phytomedicine*  
569 2019; 65: 153100. <https://doi.org/10.1016/j.phymed.2019.153100>
- 570 [53] TREPAT X, CHEN Z, JACOBSON K. Cell migration. *Compr Physiol* 2012; 2: 2369-2392.  
571 <https://doi.org/10.1002/cphy.c110012>
- 572 [54] YOST C, TORRES M, MILLER JR, HUANG E, KIMELMAN D, et al. The axis-inducing  
573 activity, stability, and subcellular distribution of beta-catenin is regulated in *Xenopus*  
574 embryos by glycogen synthase kinase 3. *Genes Dev* 1996; 10: 1443-1454.  
575 <https://doi.org/10.1101/gad.10.12.1443>
- 576 [55] WAN G, LIU Y, ZHU J, GUO L, LI C, et al. SLFN5 suppresses cancer cell migration and  
577 invasion by inhibiting MT1-MMP expression via AKT/GSK-3 $\beta$ / $\beta$ -catenin pathway. *Cell*  
578 *Signal* 2019; 59: 1-12. <https://doi.org/10.1016/j.cellsig.2019.03.004>
- 579 [56] MOSTAFA AM, HAMDY NM, ABDEL-RAHMAN SZ, EL-MESALLAMY HO. Effect of  
580 vildagliptin and pravastatin combination on cholesterol efflux in adipocytes. *IUBMB Life*  
581 2016; 68: 535-543. <https://doi.org/10.1002/iub.1510>
- 582 [57] ATTA H, ALZAHABY N, HAMDY NM, EMAM SH, SONOUSI A, et al. New trends in  
583 synthetic drugs and natural products targeting 20S proteasomes in cancers. *Bioorg Chem*  
584 2023; 133: 106427. <https://doi.org/10.1016/j.bioorg.2023.106427>
- 585

## 586 **Figure Legends**

587

588 **Figure 1.** Cytotoxic effects of isoguanosine (ISO) in hepatocellular carcinoma (HCC) cells. Cell

589 viability was assessed using the CCK-8 assay. A) Huh-7, HepG2, and Hep3B cells were treated with  
590 various concentrations (0, 20, 40, 60, 80, and 100  $\mu$ M) of ISO and 5-FU for 24 h. B) Cells were  
591 treated with 27  $\mu$ M ISO or 5-FU for 6, 12, 18, 24, and 30 h. C) Normal cell lines (THLE-2, IMR-90,  
592 293T, and GES-1) were treated with ISO or 5-FU at concentrations of 20-100  $\mu$ M for 24 h. D) The  
593 same cell lines were treated with 27  $\mu$ M ISO or 5-FU over a time course (6, 12, 18, 24, and 30 h).  
594 (\* $p < 0.05$ , \*\* $p < 0.01$ , \*\*\* $p < 0.001$  vs. 5-FU) E) Huh-7 cells were stained with Trypan blue and  
595 visualized using fluorescence microscopy (scale bar=50  $\mu$ m). F) Huh-7 cells were stained with  
596 Hoechst 33342 and observed by fluorescence microscopy (scale bar=50  $\mu$ m).

597

598 **Figure 2.** Network pharmacology analysis and Molecular Docking analysis of ISO against HCC. A)  
599 Chemical structure of ISO. B) Venn diagram of overlapping targets between ISO and HCC. C) PPI  
600 network constructed using the MCODE plugin. Nodes with a higher number of connections  
601 represent core components. D) KEGG pathway enrichment analysis. E-G) GO enrichment analyses  
602 showing biological processes (BP), molecular functions (MF), and cellular components (CC). H)  
603 Results of ISO with AKT1, CASP3, and GSK3B.

604

605 **Figure 3.** Apoptotic effects of ISO in Huh-7 cells were treated with 27  $\mu$ M ISO for 0, 3, 6, 12, and  
606 24 h. A) Apoptosis in Huh-7 cells was visualized using Annexin V-FITC/PI staining and  
607 fluorescence microscopy (scale bar=50  $\mu$ m). B) Apoptotic cell percentage was measured via flow  
608 cytometry. C) Changes in mitochondrial membrane potential (MMP) were assessed by flow  
609 cytometry. D) Apoptotic protein expression levels were analyzed using western blotting. E)  
610 Expression of p-ERK, p-JNK, p-p38, and p-STAT3 was evaluated by western blotting. F-H) Huh-7  
611 cells treated with 27  $\mu$ M ISO and 10  $\mu$ M MAPK signaling pathway inhibitors for 24 h. Quantitative  
612 analysis of Western blotting in F-H results is shown in Supplementary Figure S2.  $\alpha$ -tubulin was  
613 used as a loading control.

614

615 **Figure 4.** Effects of ISO on reactive oxygen species (ROS) accumulation in Huh-7 cells. A) ROS  
616 levels were detected by fluorescence microscopy. B) ROS levels in Huh-7 cells treated with 27  $\mu$ M  
617 ISO and/or 10 mM N-acetyl cysteine (NAC) for 24 h. C) Flow cytometry analysis of intracellular  
618 ROS levels. D) Apoptosis levels in Huh-7 cells treated with ISO and/or NAC for 24 h, measured by

619 flow cytometry. E) Western blotting analysis of p-ERK, p-JNK, p-p38, p-STAT3, cle-casp-3, and  
620 cle-PARP expression.  $\alpha$ -tubulin was used as the internal reference protein.

621

622 **Figure 5.** Effects of ISO on cell cycle in Huh-7 cells were treated with 27  $\mu$ M ISO for 0, 3, 6, 12,  
623 and 24 h. A) Fluorescence microscopy analysis of Ki67-stained Huh-7 cells. B) Cell cycle  
624 distribution was analyzed via flow cytometry. C) Flow cytometry assessment of cell cycle  
625 progression in cells treated with ISO and/or NAC. D) Western blot analysis of G2/M-related  
626 proteins. E) ISO and/or NAC treatment for 24 h. F) ISO and/or AKT inhibitor (HY10249) treatment  
627 for 24 h.  $\alpha$ -tubulin was used as a loading control.

628

629 **Figure 6.** Effects of ISO on cell migration in Huh-7 cells were treated with 27  $\mu$ M ISO for 0, 3, 6,  
630 12, and 24 h. A) Transwell assay for migratory ability (scale bar=100  $\mu$ m). B) Transwell assay  
631 following treatment with ISO and/or NAC for 24 h. (C) Cell migration assay assessing motility  
632 (scale bar=100  $\mu$ m). D) Migration assay after ISO and/or NAC treatment for 24 h. E) Western  
633 blotting of migration-associated proteins. F) ISO and/or NAC treatment for 24 h. G) ISO and/or  
634 HY10249 treatment for 24 h.  $\alpha$ -tubulin served as the internal reference.

635

636 **Figure 7.** Schematic diagram of the anticancer mechanisms of ISO in Huh- 7 cells. ISO triggers the  
637 accumulation of ROS, which mediates the regulation of multiple signaling pathways. 1. Apoptosis  
638 induction: ROS activates MAPK signaling (ERK, JNK, p38), leading to the inhibition of STAT3,  
639 downregulation of Bcl- 2, upregulation of Bad, and subsequent activation of the caspase- 3/PARP  
640 apoptotic cascade. 2. Cell cycle arrest: ROS suppresses the AKT pathway, resulting in the  
641 upregulation of p21 and p27, and the downregulation of CDK1/2 and Cyclin B, thereby arresting  
642 the cell cycle. 3. Migration inhibition: ROS inhibits AKT, which inactivates GSK-3 $\beta$ , leading to the  
643 downregulation of  $\beta$ -catenin, upregulation of E- cadherin, and downregulation of N- cadherin,  
644 ultimately inhibiting cell migration. These effects collectively contribute to the anti- cancer activity  
645 of ISO in HCC cells.

Fig. 1 [Download full resolution image](#)

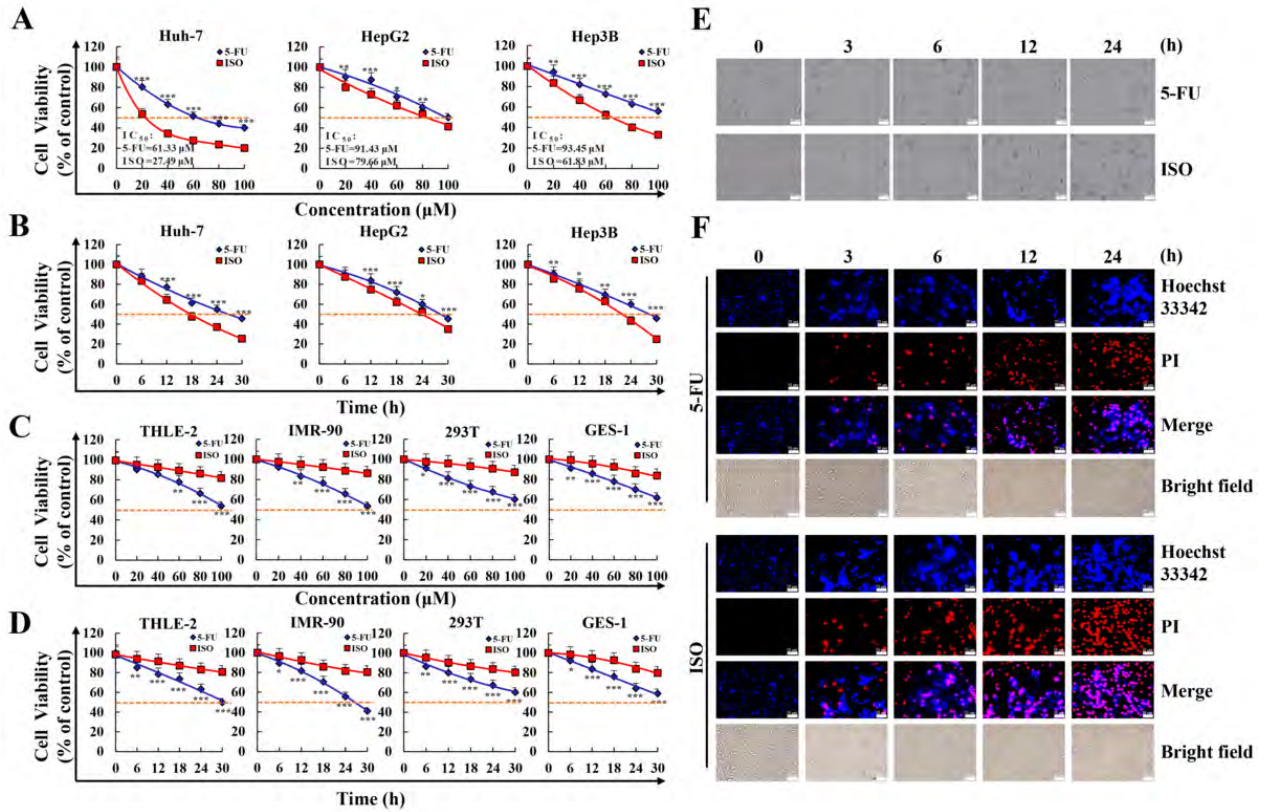


Fig. 2 [Download full resolution image](#)

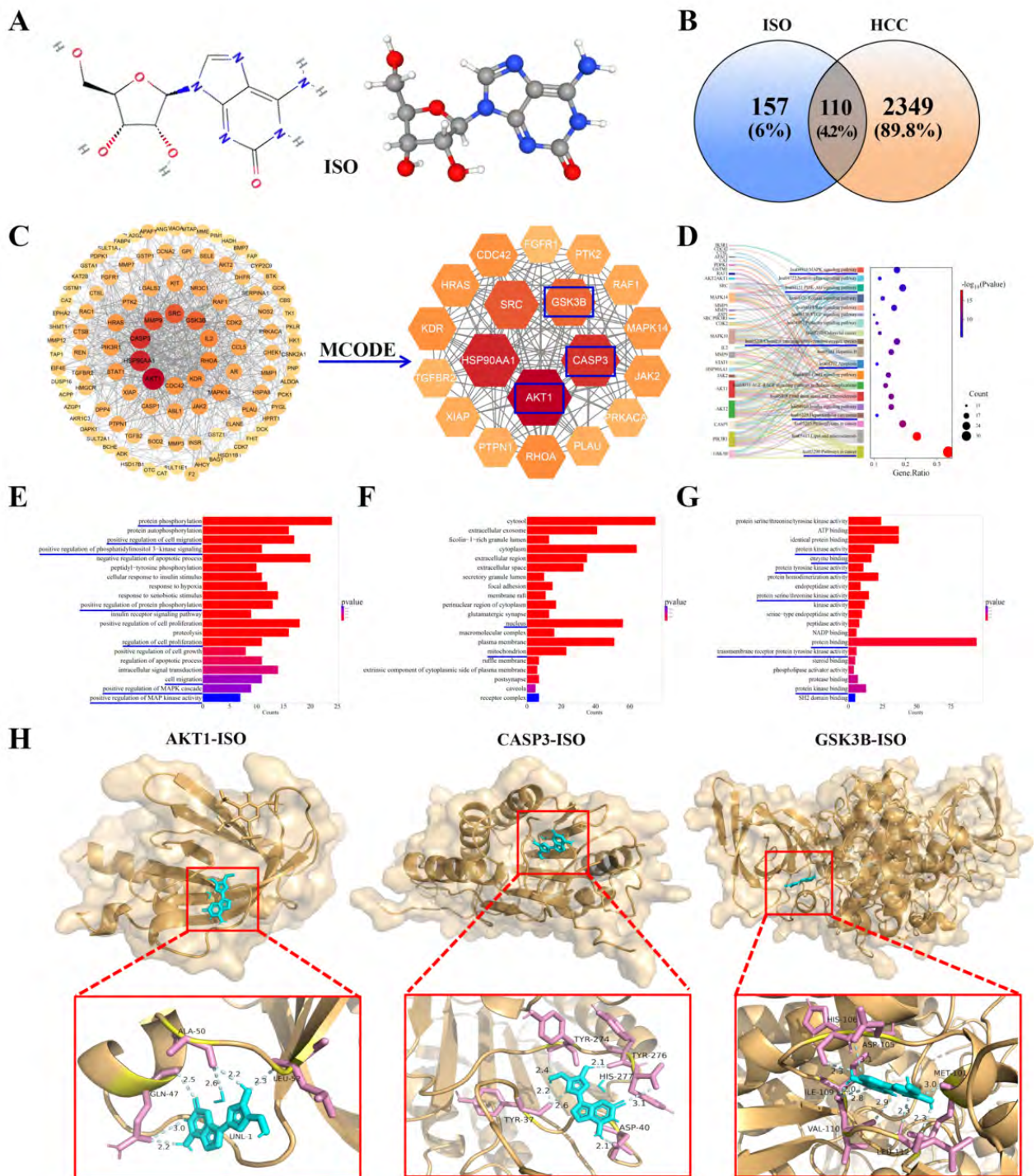


Fig. 3 [Download full resolution image](#)

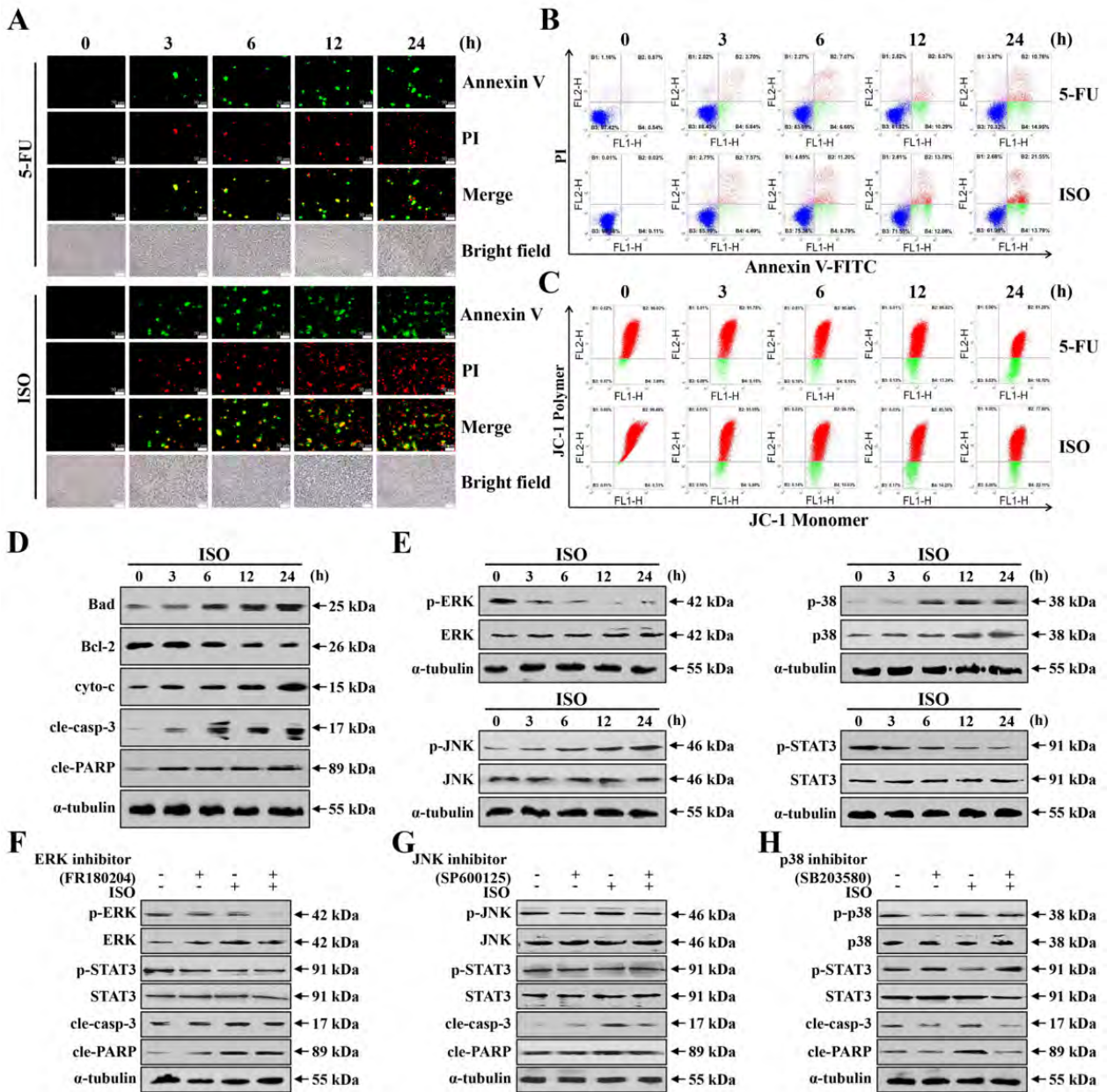


Fig. 4 [Download full resolution image](#)

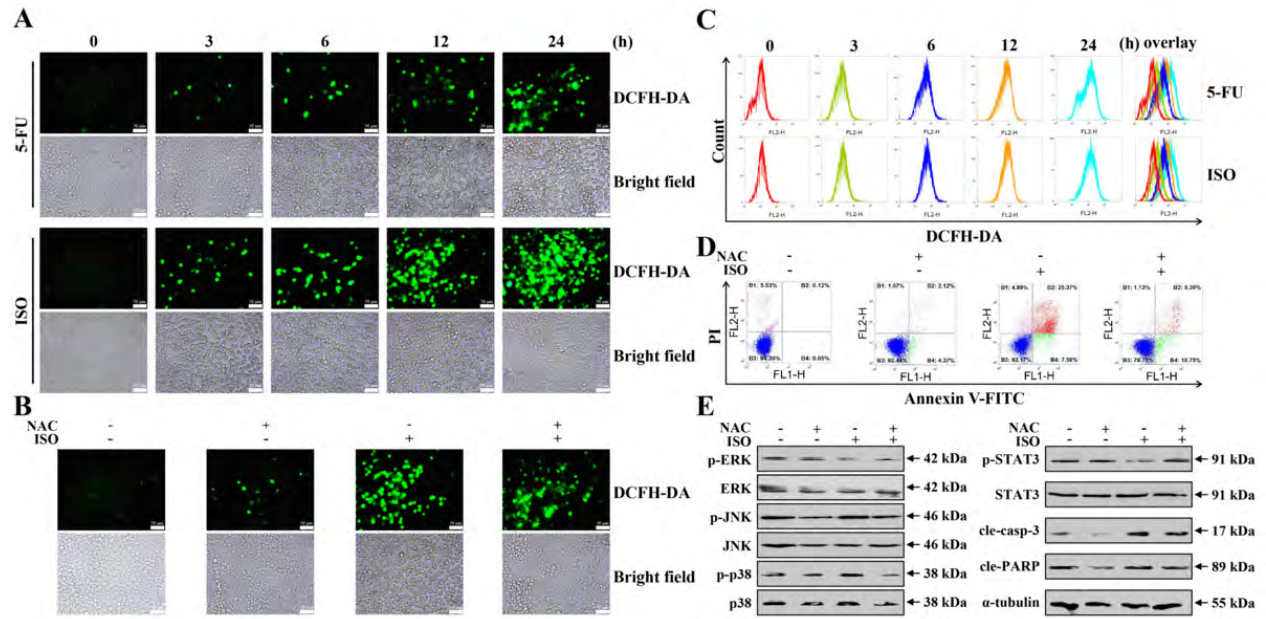


Fig. 5 [Download full resolution image](#)

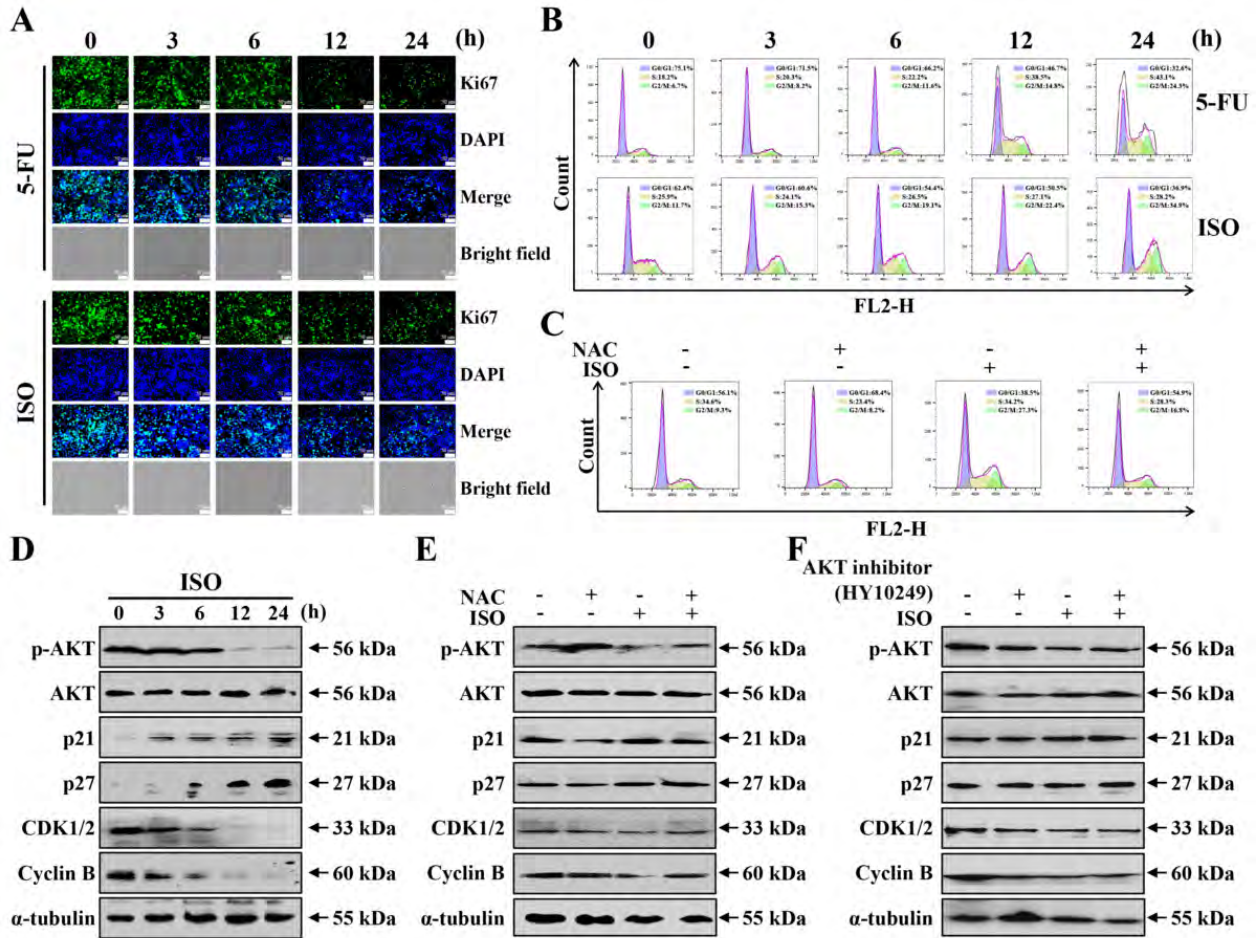


Fig. 6 [Download full resolution image](#)

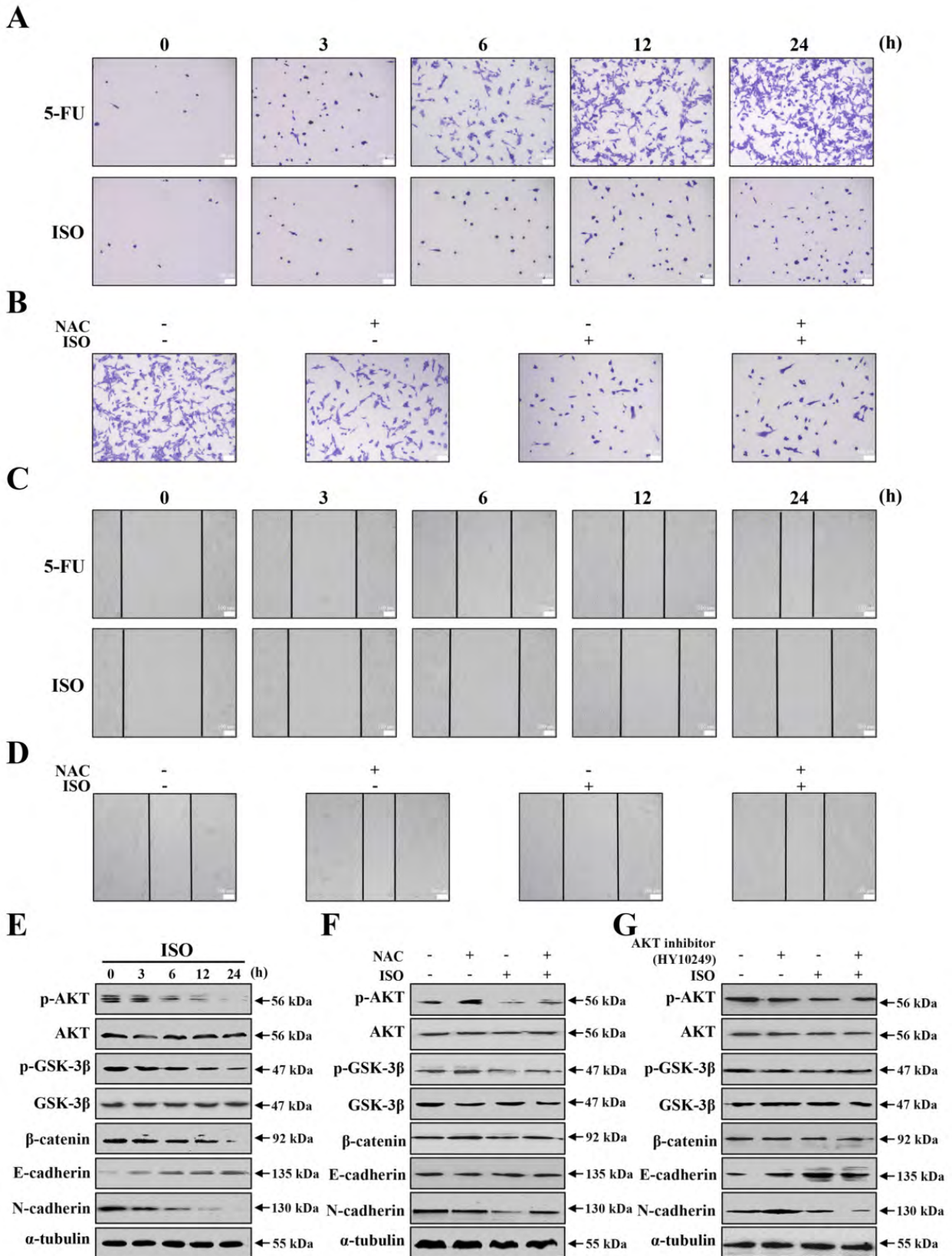


Fig. 7 [Download full resolution image](#)

